NeuroImage: Clinical 7 (2015) 28–33

Contents lists available at ScienceDirect

NeuroImage: Clinical

journal homepage: www.elsevier.com/locate/ynicl

The relationship between regional microstructural abnormalities of the corpus callosum and physical and cognitive disability in relapsing–remitting multiple sclerosis

Maria Eugenia Caligiuri[a], Stefania Barone[b], Andrea Cherubini[a,*], Antonio Augimeri[a], Carmelina Chiriaco[a], Maria Trotta[b], Alfredo Granata[b], Enrica Filippelli[b], Paolo Perrotta[a], Paola Valentino[b], Aldo Quattrone[a,b]

[a]Neuroimaging Unit, Institute of Molecular Bioimaging and Physiology, National Research Council (IBFM-CNR), Viale Europa, Germaneto, Catanzaro 88100, Italy
[b]Institute of Neurology, University "Magna Graecia", Germaneto, Catanzaro 88100, Italy

ARTICLE INFO

Article history:
Received 30 July 2014
Received in revised form 6 November 2014
Accepted 12 November 2014
Available online 18 November 2014

Keywords:
Multiple sclerosis
Multimodal MRI
Corpus callosum
Disability
Cognitive impairment

ABSTRACT

Significant corpus callosum (CC) involvement has been found in relapsing–remitting multiple sclerosis (RRMS), even if conventional magnetic resonance imaging measures have shown poor correlation with clinical disability measures. In this work, we tested the potential of multimodal imaging of the entire CC to explain physical and cognitive disability in 47 patients with RRMS. Values of thickness, fractional anisotropy (FA) and mean diffusivity (MD) were extracted from 50 regions of interest (ROIs) sampled along the bundle. The relationships between clinical, neuropsychological and imaging variables were assessed by using Spearman's correlation. Multiple linear regression analysis was employed in order to identify the relative importance of imaging metrics in modeling different clinical variables. Regional fiber composition of the CC differentially explained the response variables (Expanded Disability Status Scale [EDSS], cognitive impairment). Increases in EDSS were explained by reductions in CC thickness and MD. Cognitive impairment was mainly explained by FA reductions in the genu and splenium. Regional CC imaging properties differentially explained disability within RRMS patients revealing strong, distinct patterns of correlation with clinical and cognitive status of patients affected by this specific clinical phenotype.

1. Introduction

Multiple sclerosis (MS) is a complex and clinically heterogeneous inflammatory demyelinating disease of the central nervous system that often results in marked physical and cognitive impairment. During the course of the disease, the tissue of the entire central nervous system is affected by demyelination, axonal damage, gliosis, inflammation and, sometimes, remyelination, which cannot be clearly distinguished *in vivo* by conventional MRI (Schmierer et al., 2007). The corpus callosum (CC) is the largest white matter bundle in the human brain and has been found affected by lesions in up to 53% of MS patients (Barnard and Triggs, 1974; Gean-Marton et al., 1991; Lumsden, 1971; Simon et al., 1986). Given its size and the strong directionality of its fibers, CC is one of the few white matter tracts that can be identified with low uncertainty by quantitative MRI and diffusion tensor imaging (DTI), which allow the study of its macro- and microstructures respectively. Although it is well known that CC damage progresses along the course of MS (Pelletier et al., 2001), studies on the correlation between bundle abnormalities and disability have led to inconsistent results (Hasan et al., 2005; Sigal et al., 2012; Rimkus et al., 2013; Ozturk et al., 2010; Yaldizli et al., 2014). To our knowledge, the majority of these studies adopted metrics averaged on *a priori* subdivisions of the CC to investigate its involvement in MS. Given the limited correlation previously found between MRI measures of the CC and physical and cognitive disability, we hypothesized that a stronger relationship could be uncovered by analyzing region-specific callosal changes, detected by multimodal MRI. Our assumption was that, without any *a priori* constraint upon the topography of the bundle, macro- and micro-structural abnormalities might yield complementary information about disability in a cohort of patients with a relapsing–remitting course of MS (RRMS).

2. Materials and methods

2.1. Patients

Forty-seven consecutive patients with a diagnosis of RRMS according to the 2010 revised McDonald criteria (Polman et al., 2011) were involved in this study. Inclusion criteria were absence of clinical relapses

* Corresponding author at: CNR-URT, University "Magna Graecia", Viale Europa, Germaneto, Catanzaro 88100, Italy. Tel.: +39 09613695901; fax: +39 09613695919.
E-mail address: mariaeugenia.caligiuri@gmail.com (M.E. Caligiuri), stefania.barone@hotmail.it (S. Barone), andrea.cherubini@cnr.it (A. Cherubini), augimeriantonio@gmail.com (A. Augimeri), carmenchiriaco@alice.it (C. Chiriaco), mariatrotta2007@libero.it (M. Trotta), alf.granata@gmail.com (A. Granata), enrica.filippelli@libero.it (E. Filippelli), pperrotta5@gmail.com (P. Perrotta), p.vale@unicz.it (P. Valentino), quattrone@unicz.it (A. Quattrone).

http://dx.doi.org/10.1016/j.nicl.2014.11.008

in the month before the MRI scan and assumption of a first-line disease modifying therapy (Interferon-beta or Glatiramer acetate). Since mechanisms by which disease-modifying agents may act on the brain are not fully understood (Zivadinov et al., 2008), we chose to homogenize our sample in terms of immuno-modulating therapy, to exclude confounding effects on MRI measures that could be triggered by medications and not only by MS pathology. Other exclusion criteria were: evidence of major depression or other psychiatric disorders; past or current history of traumatic brain injury or other coexisting medical disorders; consumption of antidepressant, anxiolytic, antipsychotic or antiepileptic drugs; and consumption of steroids in the month before the neuropsychological testing, since these substances may influence cognitive performance. On the same day of the MRI acquisition, in all participants physical disability was assessed by the Expanded Disability Status Scale (EDSS) score while cognitive and executive functions were explored through the Brief Repeatable Battery of Neuropsychological Tests and the Stroop test, administered by an expert (C.C.) with more than 10 years of experience in MS. The following domains were explored: a) verbal memory: Long Term Storage, Consistent Long Term Recall, and Selective Reminding Test Delayed; b) language: Word List Generation; c) visuo-spatial memory: Spatial Recall Test (Immediate and Delayed); and d) executive functions: Symbol Digit Modalities Test and Stroop Test. Cut-off values for each test were extracted by previously published normative data on the Italian population (Amato et al., 2006). In order to define the degree of neuropsychological impairment, an overall cognitive score was determined for each patient as the number of failed tests.

All participants provided written informed consent and the study was approved by the institutional review board.

2.2. MRI acquisition and processing

All participants underwent the same MRI scanning protocol. Patients were examined using a 3-Tesla GE MR750 scanner (GE Healthcare, Rahway, NJ). The MRI protocol included whole-brain, three-dimensional, T1-weighted (BRAVO), spoiled gradient recall echo (TE/TR = 3.7/9.2 ms, flip angle 12°, voxel size = $1 \times 1 \times 1$ mm^3); DTI (b = 0, 1000; diffusion weighting along 27 non-collinear gradient directions; matrix size 128×128; 80 axial slice; number of b0 images = 4; NEX = 2; voxel size = $2 \times 2 \times 2$ mm^3); and fast fluid-attenuated inversion-recovery (FLAIR) axial images (TR = 9500 ms, TE = 100 ms; matrix size 512×512, FOV: 24 cm; 36 slices, 4 mm slices, 0 mm gap). Image processing was performed using the Functional Magnetic Resonance Imaging of the Brain (FMRIB) Analysis Group Software Library (FSL) (Oxford University, United Kingdom). Image distortions induced by eddy currents and head motion in the DTI data were corrected by applying a 3D full affine (mutual information cost function) alignment of each image to the mean no diffusion weighting (b0) image. After distortion corrections, DTI data were averaged and concatenated into twenty-eight (1 mean b0 + 27 b1000) volumes. A diffusion tensor model was fit at each voxel, generating fractional anisotropy (FA) and mean diffusivity (MD) maps. The FA maps created were then registered to brain-extracted whole-brain volumes from T1-weighted images using a full affine (correlation ratio cost function) alignment with nearest-neighbor resampling. The calculated transformation matrix was then applied to the MD maps with identical resampling options. Normal appearing CC was manually segmented by two experts (P.P. and A.G.) on the midsagittal plane of T1-weighted images, and subsequently averaged on a consensus binary mask. To accurately and automatically extract the bundle thickness profile we used an approach recently proposed by Adamson et al. (2011). Briefly, the thickness model was derived by computing a solution to Laplace's equation evaluated on callosal voxels. The streamlines from this solution formed non-overlapping, cross-sectional contours, the lengths of which were modeled as the callosal thickness. A smooth center line, obtained with cubic spline interpolation between measurement points, was divided into 51 regions of interest (ROIs) of equal lengths by 50 nodes. At each node, the distance of the line extending orthogonally to each boundary of the CC represented its thickness. We then extracted the values of MD and FA from the same 50 ROIs by overlaying the thickness profile onto the T1-coregistered DTI maps. At each ROI, we computed the MD/FA value as a weighted 2D Gaussian average with radius 2 mm. Manual delineation of T1 and FLAIR lesions was performed by an expert radiologist (P.P.), who traced the lesion outline with a mouse-controlled cursor by using MRIcron software (http://www.mccauslandcenter.sc.edu/CRNL). Lesion volume across whole brain, whole CC and midsagittal CC was assessed by using FSL. A graphical description of the processing workflow is shown in Fig. 1.

2.3. Statistical analysis

Spearman's correlation was tested between each of the clinical/neuropsychological variables and, in turn, each of the three imaging features from the entire CC (*i.e.*, thickness, FA, MD). Spearman's correlation was used since Shapiro–Wilk testing showed that our variables were not normally distributed. Correlation significance level was set at P = 0.05 after correcting for multiple comparisons according to the false discovery rate method (Benjamini and Hochberg, 1995). In order to understand which of the three imaging variables had a greater role in explaining clinical and cognitive status in RRMS, we performed a multivariate linear regression analysis. For each ROI of the CC, we built three different linear regression models in which thickness, MD and FA of the ROI were explanatory variables and EDSS, disease duration and cognitive performance, in turn, represented the dependent variable. Also, gender was added to the model as a covariate, since it has been shown to have an effect on disease progression (Voskuhl and Gold, 2012). In each model (*i.e.*, on each ROI of the bundle) we identified the explanatory variable that better described the response variable by comparing the regression coefficients. To take into account the influence of MS lesions, regression analyses were repeated adding lesion load (either total or regional) in each model as the fourth explanatory variable. Since we analyzed the entire bundle, we used the Witelson scheme as a guide to interpret results (Witelson, 1989). The topography of the CC is described by five sections, defined as arithmetic fractions of the maximum anterior–posterior extent. Section I, including the rostrum, genu, and rostral body, is crossed by fibers from the prefrontal, premotor, and supplementary motor cortical areas. Motor fibers are assumed to cross the CC through the anterior midbody (section II), whereas the somaesthetic and posterior parietal fiber bundles should cross the CC through the posterior midbody (section III). The isthmus (section IV) is assigned to the posterior parietal and superior temporal cortical areas, and the splenium (section V), is assigned to the inferior temporal, parietal, and occipital cortical regions.

3. Results

3.1. Study cohort

Demographic and clinical characteristics of the cohort are shown in Table 1. Thirteen patients (27.7%) failed at least three out of nine neuropsychological tests and were considered cognitively impaired.

3.2. Correlation analysis between clinical and neuropsychological variables and structural and diffusion properties of the CC

As shown in Fig. 2, correlation between EDSS and thickness was largely significant in the anterior midbody (section II, r values ranging from −0.50 to −0.63, P < 0.05). The significance pattern for MD and FA showed significant correlation in the splenium (section V; MD only: r values ranging from 0.42 to 0.44, P < 0.05), in section II (FA: r values ranging from −0.46 to −0.49, P < 0.05; MD: r values ranging from 0.49 to 0.59, P < 0.05) and in section I (FA: r values ranging from −0.38 to −0.45, P < 0.05; MD: r values ranging from 0.52 to 0.59,

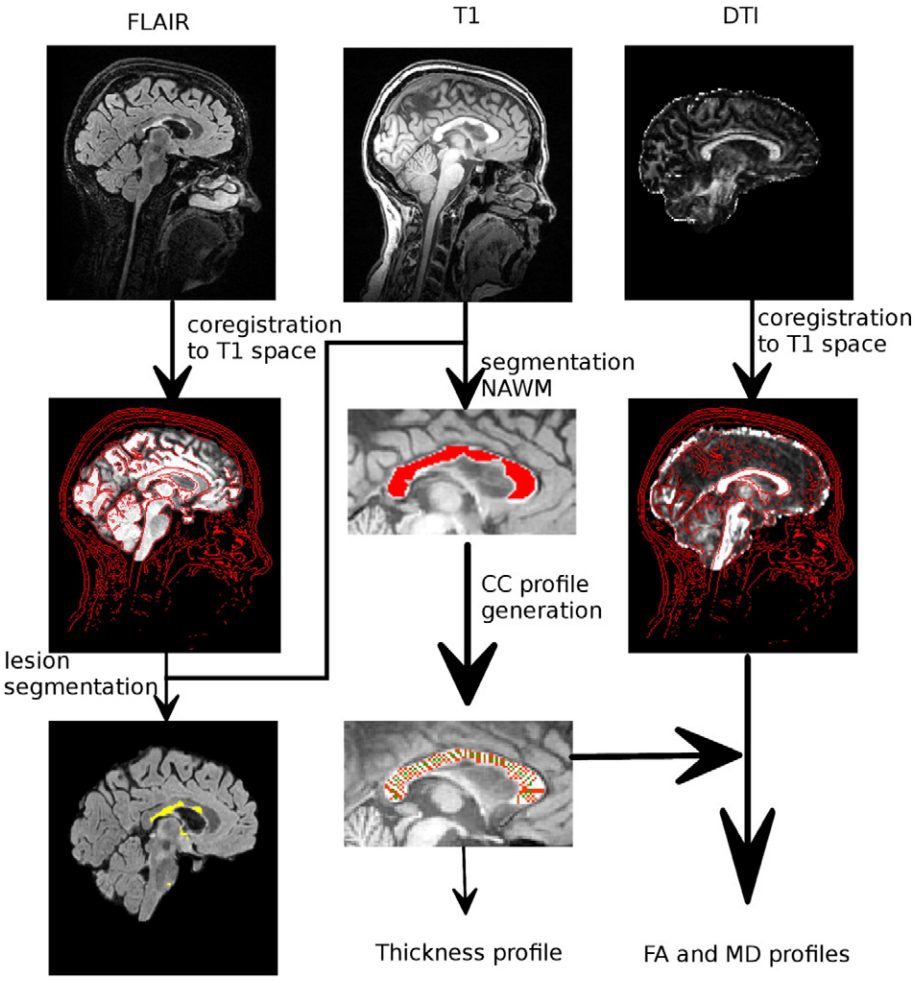

Fig. 1. Image processing workflow. FLAIR: fluid attenuated inversion recovery; DTI: diffusion tensor imaging; NAWM: normal-appearing white matter; CC: corpus callosum; FA: fractional anisotropy; MD: mean diffusivity.

Table 1
Demographic, clinical and neuropsychological characteristics of the cohort.

Subjects, n	47
Course of disease	RRMS
Median age, y (range)	34 (21–61)
Female, %	60
Age at onset, y (SD)	27.5 (7.2)
Disease duration, mo (SD)	97.7 (80.9)
Education, y (SD)	11.6 (3.2)
Median EDSS score (IQR)	2.0 (2.0–4.0)
DMT	IFN-B/GLAT
Whole-brain lesion volume, mm^3 (SD)	17,851.2 (14,917.9)
Mean MMSE (SD)	29.0 (1.4)
LTS; mean (SD)	37.1 (13.5)
CLTR; mean (SD)	27.1 (11.8)
SRTD; mean (SD)	6.3 (2.5)
SPART-I; mean (SD)	17.5 (4.9)
SPART-D; mean (SD)	5.8 (2.4)
WLG; mean (SD)	16.0 (4.2)
SDMT; mean (SD)	38.1 (12.2)
STROOP-C; mean (SD)	37.8 (9.5)
STROOP-CW; mean (SD)	18.7 (6.0)
Cognitive score, median number of failed tests (range)	2 (0–7)

Abbreviations: RRMS = relapsing–remitting multiple sclerosis; SD = standard deviation; EDSS = Expanded Disability Status Scale; DMT = Disease Modifying Therapy; IFN-B/GLAT = Interferon-beta/Glatiramer acetate; MMSE = Mini Mental State Examination; LTS = Long Term Storage; CLTR = Consistent Long Term Recall; SRTD = Selective Reminding Test Delayed; SPART-I = Spatial Recall Test Immediate; SPART-D = Spatial Recall Test Delayed; WLG = Word List Generation; SDMT = Symbol Digit Modalities Test; STROOP-C = Stroop Color Task; STROOP-CW = Stroop Color–Word Task; IQR = interquartile range.

$P < 0.05$). Disease duration showed a differential pattern of correlation along the bundle thickness profile: we found that correlation was most significant across section III (r values ranging from −0.39 to −0.49, $P < 0.05$) and sections IV–V (r values ranging from −0.38 to −0.46, $P < 0.05$), while barely significant in section I (r values ranging from −0.38 to −0.39, $P < 0.05$), according to Witelson's classification. Correlation significance between duration and MD was not significant. Instead, correlation with FA was significant in section I (r values ranging from −0.36 to −0.44, $P < 0.05$) and section V ($r = -0.38$, $P < 0.05$). The cognitive score correlated with all the imaging variables along the whole bundle, revealing peaks of significant correlation with thickness in section I (r values ranging from −0.46 to −0.59, P values < 0.05), with FA in sections I and IV (I: r values ranging from −0.46 to −0.55, $P < 0.05$; IV: r values ranging from −0.44 to −0.55, $P < 0.05$) and with MD across sections III and IV (III: r values ranging from 0.46 to 0.51, $P < 0.05$; IV: r values ranging from 0.42 to 0.52, $P < 0.05$) and in section I (r values ranging from 0.43 to 0.50, $P < 0.05$).

3.3. Regression analysis

As shown in Fig. 3, multivariate linear regression analysis confirmed the spatially heterogeneous relationship between key variables of RRMS disability and multimodal imaging characteristics of the entire CC. In particular, when considering only thickness, MD, and FA as independent variables, relationship with EDSS in sections II and IV was mainly guided by thickness, while MD gave significant contributions to model variance

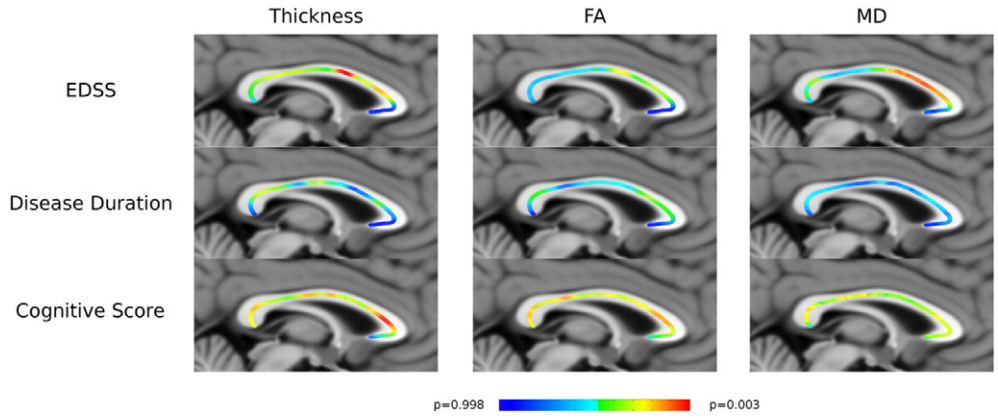

Fig. 2. Significance of Spearman's correlation between the three main disease variables (EDSS, disease duration, cognitive score) and each of the imaging metrics (thickness, FA, MD) measured along the entire CC; on the color map, green corresponds to the significance threshold P = 0.05, corrected for multiple comparisons with false discovery rate approach.

in sections I and III. FA contributions were barely present only in region I. Relationship between the bundle and disease duration highlighted a significant contribution from thickness in sections II and IV, from MD in the splenium and from FA in the anterior third. When modeling cognitive score, instead, FA contributed consistently in section I and to a less extent in region IV, combined with MD in sections III and V, and with thickness in the rostrum. We repeated the analysis by adding lesion volume as explanatory variable. We used lesion volume both in whole white matter and in a callosal ROI centered on the midsagittal CC section: since results were very similar, we reported only those relative to the whole-brain lesion load. By including lesion volume in the analysis, the relative importance of the independent variables in explaining the variance of each model remained roughly unchanged and, as expected, the insertion of lesion load increased the overall variance explained by the models.

4. Discussion

In the present study, we have analyzed microstructural abnormalities across the entire CC in RRMS patients. To the best of our knowledge, this is the first study correlating callosal fiber thickness, MD and FA in different CC ROIs with disability. In contrast to the majority of studies, we carried out the analysis without imposing any *a priori* subdivision on the bundle. Astonishingly, the ROIs significantly involved in explaining disability were naturally matched to the functional sections described by Witelson (1989) and to the fiber composition of the bundle observed

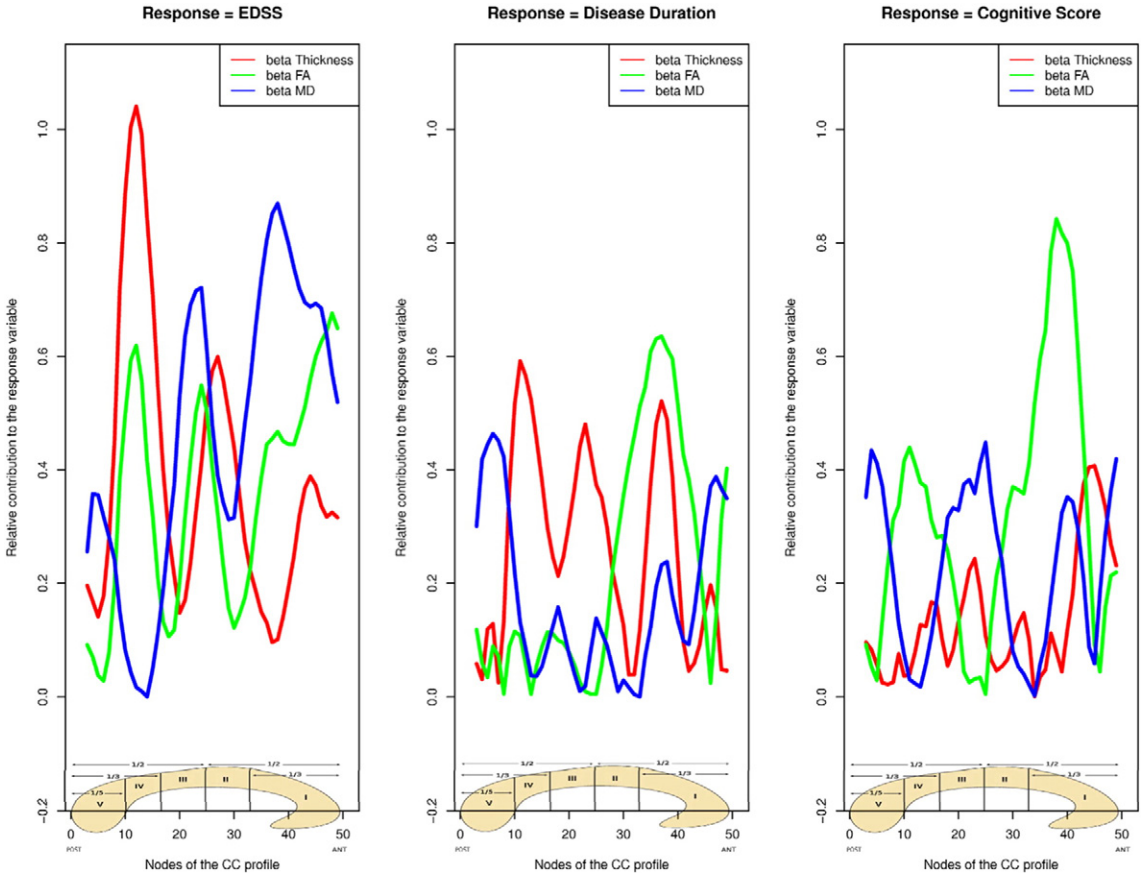

Fig. 3. Regression coefficients of the imaging variables acting as predictors in the multivariate analysis. A graphical representation of the Witelson classification is shown on the x-axis to highlight *post-hoc* correspondence between each predictor's contribution in explaining the clinical response variable and the different fiber classes of the bundle.

by Aboitiz et al. (1992), which were used only as a guide during the *post-hoc* interpretation of results. In particular, associations between physical and cognitive disability and structural abnormalities were spatially segregated. Previous studies had discovered progressive damage of the CC in MS patients compared to controls (Pelletier et al., 2001), but findings about the relationship between the bundle and disease variables have been rather inconsistent, ranging from no relationship at all (Hasan et al., 2005) to modest associations (Sigal et al., 2012; Rimkus et al., 2013) mainly with interhemispheric dysfunction measures rather than clinical disability variables (Pelletier et al., 2001; Ozturk et al., 2010; Yaldizli et al., 2014), or among different disease courses (Pelletier et al., 2001; Hasan et al., 2005; Sigal et al., 2012; Rimkus et al., 2013; Ozturk et al., 2010; Yaldizli et al., 2014). Furthermore, to our knowledge, none had yet modeled clinical variables through continuous imaging features within RRMS only. We believe that, in this framework, it is possible to study the specific disease course without the influence of those mechanisms that promote progression to other courses.

4.1. Correlation findings

Disease duration was associated with bundle thickness, which is in line with different other studies confirming that atrophy progresses along the course of the disease (Pelletier et al., 2001). As expected, EDSS score, which measures physical disability, correlated with regions of the bundle crossed by motor and premotor fibers. The cognitive score, on the other hand, correlated with CC properties of those ROIs crossed by fibers from the prefrontal, temporal and parietal cortical areas, which are all interconnected in order to exploit higher-level brain functions. We believe that the highly significant correlations, discrepant with respect to previous research (Hasan et al., 2005; Sigal et al., 2012; Rimkus et al., 2013), might be largely explained by the fact that we assessed CC damage in a continuous fashion, without recurring to *a priori* subdivisions, and consequently to metrics averaged over predetermined sections, which might have led to loss of space-variant information.

4.2. Regression findings

Multiple regression analyses uncovered the differential pattern of contributions from the imaging characteristics of the entire CC to the global measures of disease severity. Disease duration was mainly explained by reductions in bundle thickness over the sections crossed by sensorimotor and temporo-parietal fibers, by MD increases in regions corresponding to occipital fibers and by FA decreases in prefrontal fibers. It is known from the literature (Aboitiz et al., 1992) that small fibers are densely distributed in the genu and to some extent in the splenium, while large myelinated fibers are mainly found in the body. In the light of this, the significant contribution to the model of disease duration carried by MD and FA rather than thickness of prefrontal and occipital fibers could be interpreted as an early marker of fiber damage that has not yet resulted in macroscopic atrophy, due to the large number of fibers with a small diameter that populate those regions of the CC. On the contrary, atrophy was more evident where there was loss of large, heavily myelinated axons (motor fibers). Regression models of EDSS showed that thickness reductions in the splenium and in motor areas, together with MD increases in the prefrontal and sensory areas, gave the most significant contributions to the model of physical disability. As shown in Fig. 3, by comparing the models of duration and physical disability, it can be seen that the beta coefficients relative to disease duration assume smaller values. This is in line with the evidence that there is no direct correspondence between disease duration and disease severity (Fisniku et al., 2008). Finally, when modeling cognitive impairment, FA gave the most consistent contribution to the analysis in the regions crossed by prefrontal and temporal fibers, thus suggesting damage of fibers involved in executive function and memory circuits, while MD contributed in sections related to somatosensory and occipital fibers.

4.3. Possible application in clinical trials

Since trials of potential neuroreparative agents are increasingly important in the spectrum of MS research, the need for appropriate imaging markers has been recently pointed out (Mallik et al., 2014). These measures should be computationally lean to obtain from MR images, should be sensitive and specific to myelin and, of course, should be reproducible and clinically meaningful. In this context, we believe that the present analysis method could be a convenient MRI marker in a clinical trial, from several points of view. First, it is computationally lean and reproducible: in fact, although in this testing phase it has been applied on manual segmentation of the CC, the entire analysis can be easily automated (Adamson et al., 2014). Second, our results are coherent and show meaningful clinical relationships. Third, DTI metrics extracted continuously from the CC might indirectly bring information on demyelination/remyelination. Despite the well-known limitations of diffusion-tensor modeling, these affect the DTI metrics mainly when fiber orientation per voxel cannot be correctly estimated, which should not be frequent when dealing with highly directional structures like the CC. Even taking into account DTI pitfalls, novel methods for a better reconstruction of fiber orientation are currently being implemented and could be easily integrated in our analysis (for a comparison of most recently developed methods see Daducci et al., 2014). Last, but not least, we believe that the CC might represent a crucial structure for monitoring the effects of neuroreparative drugs because of the varied nature of the fibers that form it. Damage or repair to its different regions, as measured with this convenient marker, might bring further insights not only on the integrity of callosal fibers, but also, indirectly, on the status of cortical regions that these fibers connect.

For all these reasons and from a wider perspective, continuous measures of callosal macro- and micro-structural integrity could be adopted to monitor drug efficacy in clinical trials focusing on neurorepair in multiple sclerosis, thus improving the treatment of disability and, as a consequence, the quality of life of patients suffering from this disease.

4.4. Limitations

Although the present study displays coherent relationships it has some limitations: first, the sample size is relatively small, especially given the heterogeneity of the disease. Second, results should be confirmed by longitudinal data. For this reason future studies should foresee a follow-up stage on a larger cohort of patients. Our efforts will thus focus on the progression of damage along the individual disease course, which is especially relevant when designing new treatment strategies.

5. Conclusion

In this work, we demonstrated the ability of multimodal MRI metrics to uncover spatially coherent patterns of relationship between CC damage and RRMS disability. The lack of *a priori* subdivisions on the bundle did not preclude the discovery of associations between variables; instead, it might have strengthened our results, leading us to the conclusion that the macro- and micro-structural CC damage might be a very sensitive marker of disease progression.

Acknowledgments

This work has not been funded by any grant. The authors thank Dr. Luca Passamonti for his helpful comments regarding the manuscript. All authors declare no conflict of interest.

References

Aboitiz, F., Scheibel, A.B., Fisher, R.S., Zaidel, E., 1992. Fiber composition of the human corpus callosum. Brain Res. 598 (1–2), 143–153. http://dx.doi.org/10.1016/0006-8993(92)90178-C.

Adamson, C., Beare, R., Walterfang, M., Seal, M., 2014. Software pipeline for midsagittal corpus callosum thickness profile processing. Neuroinformatics 12, 1–20. http://dx.doi.org/10.1007/s12021-013-9212-3.

Adamson, C.L., Wood, A.G., Chen, J., et al., 2011. Thickness profile generation for the corpus callosum using Laplace's equation. Hum Brain Mapp 32 (12), 2131–2140. http://dx.doi.org/10.1002/hbm.2117421305661.

Amato, M.P., Portaccio, E., Goretti, B., et al., 2006. The Rao's brief Repeatable Battery and Stroop test: normative values with age, education and gender corrections in an Italian population. Mult. Scler. 12 (6), 787–793. http://dx.doi.org/10.1177/1352458506070933317263008.

Barnard, R.O., Triggs, M., 1974. Corpus callosum in multiple sclerosis. J. Neurol. Neurosurg. Psychiatr. 37 (11), 1259–1264. http://dx.doi.org/10.1136/jnnp.37.11.12594457618.

Benjamini, Y., Hochberg, Y., 1995. Controlling the false discovery rate: a practical and powerful approach to multiple testing. J. R. Stat. Soc. Ser B. Methodological. 289–300.

Daducci, A., Canales-Rodríguez, E.J., Descoteaux, M., et al., 2014. Quantitative comparison of reconstruction methods for intra-voxel fiber recovery from diffusion MRI. IEEE Trans Med Imaging 33 (2), 384–399. http://dx.doi.org/10.1109/TMI.2013.228550024132007.

Fisniku, L.K., Chard, D.T., Jackson, J.S., et al., 2008. Gray matter atrophy is related to long-term disability in multiple sclerosis. Ann. Neurol. 64 (3), 247–254. http://dx.doi.org/10.1002/ana.2142318570297.

Gean-Marton, A.D., Vezina, L.G., Marton, K.I., et al., 1991. Abnormal corpus callosum: a sensitive and specific indicator of multiple sclerosis. Radiology 180 (1), 215–221. http://dx.doi.org/10.1148/radiology.180.1.20526982052698.

Hasan, K.M., Gupta, R.K., Santos, R.M., Wolinsky, J.S., Narayana, P.A., 2005. Diffusion tensor fractional anisotropy of the normal-appearing seven segments of the corpus callosum in healthy adults and relapsing–remitting multiple sclerosis patients. J Magn Reson Imaging 21 (6), 735–743. http://dx.doi.org/10.1002/jmri.2029615906348.

Lumsden, C.E., 1971. The immunogenesis of the multiple sclerosis plaque. Brain Res. 28 (3), 365–390. http://dx.doi.org/10.1016/0006-8993(71)90052-74939243.

Mallik, S., Samson, R.S., Wheeler-Kingshott, C.A., et al., 2014. Imaging outcomes for trials of remyelination in multiple sclerosis. J. Neurol. Neurosurg. Psychiatr. http://dx.doi.org/10.1136/jnnp-2014-30765024769473 published online first:25 April 2014.

Ozturk, A., Smith, S.A., Gordon-Lipkin, E.M., et al., 2010. MRI of the corpus callosum in multiple sclerosis: association with disability. Mult. Scler. 16 (2), 166–177. http://dx.doi.org/10.1177/1352458509353649201423309.

Pelletier, J., Suchet, L., Witjas, T., et al., 2001. A longitudinal study of callosal atrophy and interhemispheric dysfunction in relapsing–remitting multiple sclerosis. Arch. Neurol. 58 (1), 105–111. http://dx.doi.org/10.1001/archneur.58.1.10511176943.

Polman, C.H., Reingold, S.C., Banwell, B., et al., 2011. Diagnostic criteria for multiple sclerosis: 2010 revisions to the McDonald criteria. Ann. Neurol. 69 (2), 292–302. http://dx.doi.org/10.1002/ana.2236621387374.

Rimkus, Cde.M., Junqueira, T.deF., Callegaro, D., Otaduy, M.C., Leite, C.daC., 2013. Segmented corpus callosum diffusivity correlates with the Expanded Disability Status Scale score in the early stages of relapsing–remitting multiple sclerosis. Clinics (Sao Paulo) 68 (8), 1115–1120. http://dx.doi.org/10.6061/clinics/2013(08)0924037007.

Schmierer, K., Wheeler-Kingshott, C.A., Boulby, P.A., et al., 2007. Diffusion tensor imaging of post mortem multiple sclerosis brain. Neuroimage 35 (2), 467–477. http://dx.doi.org/10.1016/j.neuroimage.2006.12.01017258908.

Sigal, T., Shmuel, M., Mark, D., Gil, H., Anat, A., 2012. Diffusion tensor imaging of corpus callosum integrity in multiple sclerosis: correlation with disease variables. J Neuroimaging 22 (1), 33–37. http://dx.doi.org/10.1111/j.1552-6569.2010.00556.x21122007.

Simon, J.H., Holtås, S.L., Schiffer, R.B., et al., 1986. Corpus callosum and subcallosal-periventricular lesions in multiple sclerosis: detection with MR. Radiology 160 (2), 363–367. http://dx.doi.org/10.1148/radiology.160.2.37261143726114.

Voskuhl, R.R., Gold, S.M., 2012. Sex-related factors in multiple sclerosis susceptibility and progression. Nat Rev Neurol 8 (5), 255–263. http://dx.doi.org/10.1038/nrneurol.2012.4322450508.

Witelson, S.F., 1989. Hand and sex differences in the isthmus and genu of the human corpus callosum. A postmortem morphological study. Brain 112 (3), 799–835. http://dx.doi.org/10.1093/brain/112.3.7992731030.

Yaldizli, Ö, Penner, I.K., Frontzek, K., et al., 2014. The relationship between total and regional corpus callosum atrophy, cognitive impairment and fatigue in multiple sclerosis patients. Mult. Scler. 20 (3), 356–364. http://dx.doi.org/10.1177/1352458513496880239597709.

Zivadinov, R., Reder, A.T., Filippi, M., et al., 2008. Mechanisms of action of disease-modifying agents and brain volume changes in multiple sclerosis. Neurol. 71 (2), 136–144. http://dx.doi.org/10.1212/01.wnl.0000316810.01120.0518606968.